Available online at www.sciencedirect.com
SCIENCE DIRECT®
ELSEVIER
Nuclear Instruments and Methods in Physics Research A 517 (2004) 180–188
NUCLEAR INSTRUMENTS & METHODS IN PHYSICS RESEARCH Section A
www.elsevier.com/locate/nima

Spectral identification of thin-film-coated and solid-form semiconductor neutron detectors

Douglas S. McGregor*, J. Kenneth Shultis

Department of Mechanical and Nuclear Engineering, Kansas State University, 318 Rathbone Hall, Manhattan, KS 66506-5205, USA

Received 26 June 2003; received in revised form 1 September 2003; accepted 14 September 2003

Abstract

Semiconductor-based solid-state neutron detectors have received considerable attention in recent years. These devices can be categorized as either thin-film-coated diode detectors or solid-form bulk detectors. There have been many attempts to fabricate boron-based solid-form detectors utilizing processing techniques similar to those frequently used to fabricate thin-film-coated diodes. Consequently, results from attempts to fabricate boron-based semiconductor neutron detectors are often misinterpreted as solid-form detectors when in fact they are functioning as common thin-film-coated diodes. In principle, boron-based solid-form detectors should be able to achieve higher efficiencies for detecting thermal neutrons than can boron-based thin-film-coated diodes, but only if they are truly operating as solid-form bulk detectors. Hence, a method to distinguish between the two devices is necessary. In this paper, it is proposed that proper interpretation of the observed differential pulse-height spectra can provide the necessary discrimination between the two types of detectors. Modeled comparisons of differential pulse-height spectra between thin-film-coated devices and solid-form devices are presented, thereby providing assistance to researchers in the field to properly interpret experimental results.

PACS: 29.40.Wk

Keywords: Neutron detector; Semiconductor detector; Radiation detector

1. Introduction

Solid-state semiconductor neutron detectors offer the advantages of low-power operation and compactness as compared to most gas-filled or scintillation neutron detectors. There are two categories of neutron semiconductor detectors, namely, thin-film-coated detectors and solid-form or bulk detectors. Both types of detectors employ neutron-induced reactions to release detectable ionizing radiation. The main difference between the two types of detectors is the location within the detector assembly where the neutron interactions occur. In thin-film-coated devices, neutron interactions occur in a sensitive film adjacent to a diode detector. By contrast, in solid-form detectors the neutron interactions occur inside the bulk detector itself. The most common reactions used for semiconductor-based thermal-neutron detectors are the $^{10}B(n,\alpha)^{7}Li$, $^{6}Li(n,\alpha)^{3}H$, and the

*Corresponding author. Tel.: +1-785-532-5284; fax: +1-785-532-7057.
E-mail address: mcgregor@ksu.edu (D.S. McGregor).

0168-9002/$ - see front matter
doi:10.1016/j.nima.2003.09.037

$^{113}Cd(n,\gamma)^{114}Cd$ reactions [1]. Boron-based devices are analyzed in the present work. The $^{10}B(n,\alpha)^{7}Li$ reaction produces the following charged particle reaction products [1]

$$^{10}B+{}^{1}_{0}n\rightarrow \begin{cases} {}^{7}Li(1.015\,MeV)+\alpha(1.777\,MeV), \\ \text{Reaction } Q\text{-value} = 2.792\,MeV \\ \text{(to ground state)}, \\ {}^{7}Li^{*}(0.840\,MeV)+\alpha(1.470\,MeV), \\ \text{Reaction } Q\text{-value} = 2.310\,MeV \\ \text{(1st excited state)} \end{cases} \quad (1)$$

which are emitted in opposite directions. For the reaction in Eq. (1), 93.7% of the reactions leave the ^{7}Li ion in its first excited state, which rapidly de-excites to the ground state ($\sim 10^{-13}$ s) by releasing a 480 keV gamma ray. The remaining 6.3% of the reactions leave the ^{7}Li ion in its ground state.

Thin-film-coated devices are fabricated by applying one or more neutron reactive films upon the surface of a semiconductor diode. The simplest form, shown in Fig. 1, is a semiconductor diode upon which a single neutron reactive film, usually composed of a boron or lithium containing material, is applied directly upon the rectifying (or blocking) junction or contact. The reactive

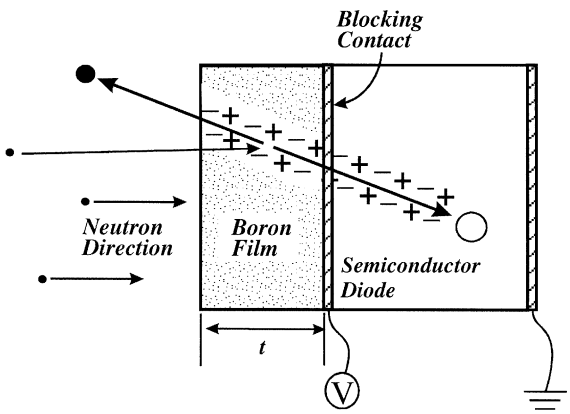

Fig. 1. The configuration of a simple thin-film-coated semiconductor diode neutron detector. The B film is applied directly to the rectifying contact surface. An applied voltage is used to drift the free charges liberated in the semiconductor diode apart, thereby producing detectable charge induction.

films can be applied using a number of different methods, including evaporation, sputtering, and chemical deposition. The diode is usually produced first, followed by the deposition of a thin coating of neutron reactive material on its surface(s). Boron- and lithium-based film coatings can range from a few thousand angstroms to several microns. When neutrons interact within the film, only one of the charged particle reaction products, which are emitted in opposite directions, may pass through the detector interface into the diode. For one of the ions to do so, the following conditions must exist [2]:

(a) The range of the reaction product ion must be greater than the distance between the interaction location and the film/detector interface.
(b) The particle trajectory must be within the solid angle subtending the film/detector interface, namely $\Omega = 2\pi[1-(x/L)]$, where x is the orthogonal distance from the reaction location to the film/detector interface and L is the reaction ion range [2].

A reaction ion entering the depletion region of the diode creates electron–hole pairs along its straight-line trajectory. Typically, diode detectors are operated in reverse bias, so that this potential causes the charge carriers to drift apart to their respective electrodes, thereby inducing a signal through their motion [2]. Since there are four possible reaction product energies released by the $^{10}B(n,\alpha)^{7}Li$ reaction, there are four different ion ranges L that must be considered for analysis. Extending the film thickness beyond the largest L does not increase the detector's efficiency because reaction products produced at distances greater than L from the diode's surface cannot penetrate the diode. In fact, due to self-absorption in the outer part of the film, the neutron detection efficiency will decrease for obverse irradiation [2]. Values of L are usually only a few microns for B solids.

Solid-form devices use a semiconductor material composed, at least partially, of a neutron reactive material. Examples of potential solid-form neutron detecting semiconductors include BN, BP, and BAs. Conceptually, such devices consist of only the B compound, upon which conductive

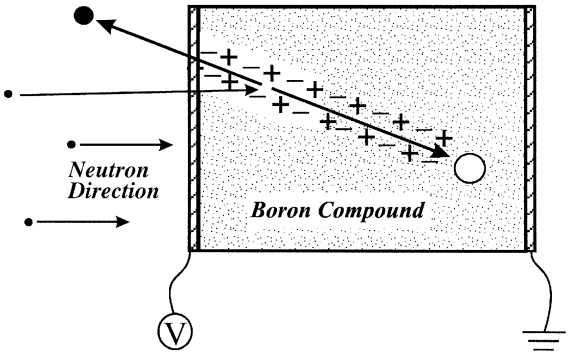

Fig. 2. The configuration of a simple solid-form (or bulk) semiconductor diode neutron detector, where the B compound performs as the detector diode. A voltage applied across the entire device is used to drift the liberated free charges apart, thereby producing detectable charge induction.

contacts have been affixed on opposite sides (see Fig. 2). The device has a voltage applied across the bulk material. Neutrons can be absorbed directly within the detector, whereupon the charged particle reaction products are released directly within the detector itself. As a result, the self-absorption and particle range problems associated with thin-film-coated diodes are not encountered with a solid-form or bulk semiconductor neutron detector. Any $^{10}B(n,\alpha)^{7}Li$ interactions in the bulk detector lead to detectable ionization. The total thermal-neutron cross-section for ^{10}B is almost all due to the (n,α) reaction and, if other elements in the boron material have negligible thermal cross-sections, the intrinsic efficiency is well approximated by

$$\varepsilon_i = 1 - \exp(-\Sigma t) \tag{2}$$

where Σ is the thermal-averaged macroscopic neutron absorption cross-section of the boron solid and t is the device thickness. In theory, a sufficiently thick device can approach 100% intrinsic efficiency for detecting thermal neutrons.

Many attractive boron semiconductors require high temperatures for traditional growth from the melt. Furthermore, these solid boron semiconductors decompose at high temperatures, and the pressures required to prevent such decomposition ultimately make melt growth of numerous boron compound semiconductors unmanageable [3,4]. Hence, boron solids, such as BP, BAs, BN, and B_4C, are generally grown by chemical vapor deposition (CVD) techniques upon a supporting substrate. Frequently, such films or layers of a boron compound are deposited upon n-type Si [3–6]. The contacts, as reported in the literature, are applied to the upper surface of the boron material and to the bottom surface of the Si substrate, as shown in Fig. 3. It should be noted that the configuration in Fig. 3 resembles the thin-film-coated diode of Fig. 1.

A more subtle resemblance of the two detector types arises from the fact that boron is a p-type

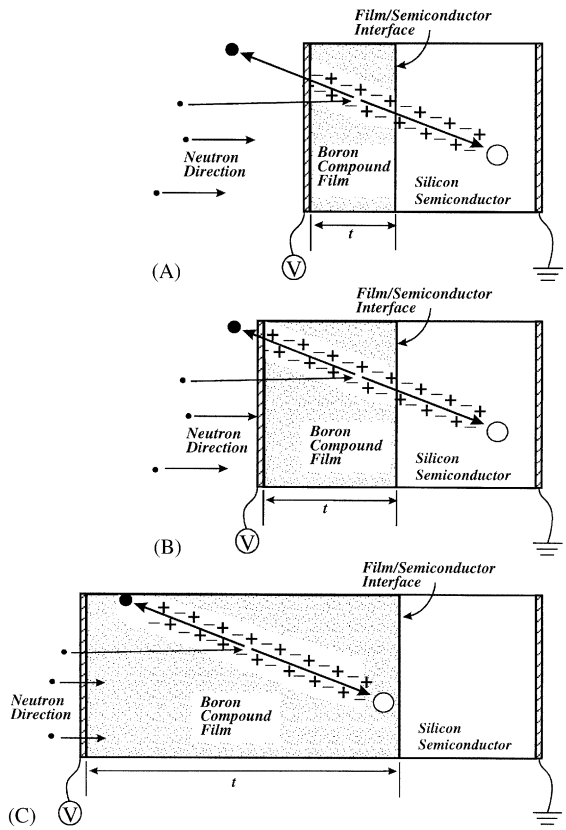

Fig. 3. The configuration commonly used to test B compound films as neutron detectors. The B compound films are often grown upon Si substrates, and a voltage is usually applied across the entire device when operated. Depicted also are three cases: (A) the B film is much thinner than the reaction product ranges, (B) the B film is nearly equivalent to either reaction product range, and (C) the B film is thicker than the combined ranges of the reaction products.

dopant in Si. Thus, growth of a boron compound upon n-type Si using elevated temperature processes, such as CVD, can produce a thin p–n junction diode at the B compound/Si interface [7,8]. It is entirely possible to misinterpret a B compound material as a functioning solid-form or bulk neutron detector, when instead a simple thin-film-coated device has been produced upon a Si p–n junction diode. Ultimately, the performance and efficiency is predetermined by which type of device has actually been fabricated. Determination of the type of solid-state neutron detector produced can be deduced through the differential pulse-height spectrum produced by the device. As shown in this paper, the pulse-height spectra obtained with each detector type are fundamentally different. Presented are modeled results establishing the expected spectral performance of both thin-film-coated and solid-form (or bulk) semiconductor neutron detectors.

The variation of the detector efficiency with the thickness of the B compound film also is remarkably different for each type of detector. In a thin-film-coated device, only one particle can enter the detector per interaction event, and due to self-absorption effects, there is an optimum coating thickness to achieve the maximum thermal-neutron detection efficiency [2]. In a solid-form device, both particles generally contribute to the pulse observed for a single interaction. As depicted in Fig. 3, thin boron coatings reduce self-absorption in a functioning thin-film-coated device [2], as well as decrease the probability that both product ions are completely absorbed in the film. In other words, the solid angles describing the intersection probability of an ion escaping the film into either the Si substrate or the region outside the film are greater for thinner films, and the solid angles describing the probability of both ions remaining entirely within the B compound film are greater for thicker films.

As the thickness of the B compound film layer is increased, the probability of full-energy absorption in the film, per reaction, increases for the solid-form device, whereas the effect of self-absorption increases for the thin-film-coated device. If the film thickness increases beyond the maximum ion range, self-absorption can actually decrease the efficiency of a thin-film-coated detector, as mentioned earlier. By contrast, the efficiency for a solid-form device always increases with increasing film thickness.

2. Model development of Monte Carlo model for pulse-height spectra

Boron carbide (B_4C), with a density of 2.52 g/cm^3 [9], was chosen as the B compound for the analysis model. Using the TRIM code [10], calculations were made to determine the energy of the four reaction product ions of Eq. (1) after passing through films of various thicknesses of B_4C and Si. For example, Fig. 4 shows the residual energy (or energy remaining) for the four reaction ions as a function of distance traveled through a B_4C film. Empirical fits were made to the TRIM data for use in the subsequent Monte Carlo simulations. These fits allow rapid calculation of energy lost and remaining energy of the ions after traveling an arbitrary distance.

A simple Monte Carlo procedure was used to calculate the energy deposited by the reaction ions of Eq. (1) in the B_4C layer and also in an adjacent silicon substrate layer. Both the B_4C and Si layers were modeled by laterally infinite slabs. A thermal-neutron beam was assumed to be uniformly and normally incident on the front face of the B_4C

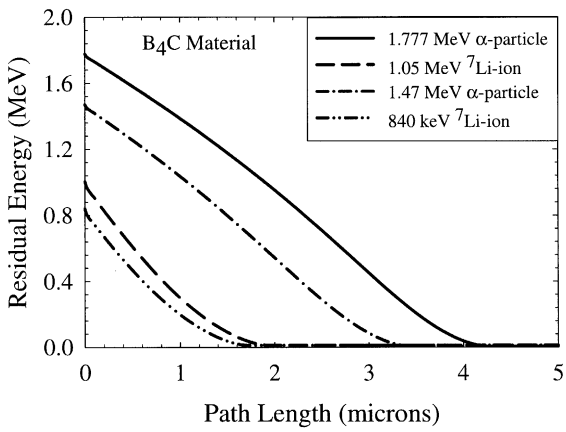

Fig. 4. The residual energy for $^{10}B(n,\alpha)^7Li$ reaction products as a function of transit distance through B_4C.

layer and to be exponentially attenuated as it traversed the B_4C layer, i.e., $I(x) = I(0)\exp(-\Sigma x)$, where $I(x)$ is the thermal-neutron intensity at depth x from the front surface of the B_4C layer and Σ is the thermal-averaged macroscopic absorption cross-section for the boron in the B_4C layer. The model in its present form assumes no distortions from edge effects. However, edge effects become important only for small devices, typically of area less than 500 μm × 500 μm square, thereby validating the simplifying assumption.

The simulation of each $^{10}B(n,\alpha)^7Li$ reaction in the B_4C layer began with the selection of a random depth x_i for the reaction where the x_i are distributed exponentially as $f(x_i) = C\exp(-\Sigma x_i)$. Here C is a normalization constant to make $f(x)$ a proper probability distribution function (pdf). The type of reaction was then randomly chosen to produce, on average, the corrected branching ratio between the $^{10}B(n,\alpha)^7Li$ (6.3%) and the $^{10}B(n,\alpha)^7Li^*$ (93.7%) reactions. A random direction for the alpha particle was then chosen from an isotropic emission pdf (the Li ion direction always being opposite to that of the alpha particle). Ions were assumed to travel in straight lines along their initial emission directions. The distances from the reaction site to the two surfaces of the B_4C layer were then calculated and the residual energies (if any) of the ions leaving the B_4C layer were computed from the empirical correlation of residual energy versus path length traveled for each ion type. The energy E_B deposited by the He and Li ions in the B_4C layer and energy E_0 of any ion entering the silicon layer were then calculated. If an ion entered the Si layer with energy E_0, the trajectory was backtracked to find the starting position in a hypothetical *silicon* first layer to produce the same residual energy entering the second silicon layer by using the empirical residual energy versus path length correlations for silicon. The distance from this hypothetical starting point to the rear surface of the second silicon layer was then calculated. With this distance, the residual energy E_1 of the ion escaping through the rear silicon surface was determined. The energy deposited in the silicon layer was determined as $E_S = E_0 - E_1$, thereby modeling the effect of inadequate depletion widths for thin-film-coated diodes.

The deposited energies E_B and E_S were then recorded in the appropriate bins of the simulated energy-deposition spectra for the two layers. After performing the simulation for many reactions (typically many millions), ideal energy-deposition spectra were obtained.

3. Modeling experimental spectra

The spectra obtained with the above Monte Carlo simulation are "ideal" in the sense that no energy straggling, large-angle ion scattering or detector noise and resolution effects are included. To simulate multi-channel analyzer (MCA) measured spectra, which include such non-ideal effects, the ideal spectra were post-processed to introduce Gaussian averaging or smearing of the counts in each energy bin of the ideal spectra. The procedure is as follows.

Let $P(E)\,dE$ be the probability a reaction leads to the deposition of energy in dE about E. Then the number of counts N_i in channel i of the ideal spectrum is

$$N_i = N_{tot}\int_{E_i-\Delta}^{E_i+\Delta} P(E)\,dE \simeq 2\Delta N_{tot}P(E_i) \tag{3}$$

where E_i is the channel midpoint energy, 2Δ is the bin energy width, and N_{tot} is the total number of ion histories. Because of non-ideal effects, an energy deposition of E has a probability $\Re(E,E')\,dE'$ of being recorded in dE' about E'. To a first approximation, a Gaussian resolution function is assumed, i.e.,

$$\Re(E,E') = \frac{1}{\sqrt{2\pi}\sigma}\exp\left[-\frac{1}{2}\left(\frac{E-E'}{\sigma}\right)^2\right]. \tag{4}$$

The probability a reaction that deposits energy in dE about E and is then recorded in channel j of the MCA spectrum is thus

$$C_j(E)\,dE = P(E)\,dE\int_{E_j-\Delta}^{E_j+\Delta}\Re(E,E')\,dE' \tag{5}$$

so that the total number of counts in channel j of the measured spectrum is

$$\begin{aligned}\hat{N}_j &= N_{\text{tot}} \int_0^{E_{\max}} C_j(E)\,\mathrm{d}E \\ &= N_{\text{tot}} \int_0^{E_{\max}} \mathrm{d}E\, P(E) \int_{E_j-\Delta}^{E_j+\Delta} \mathrm{d}E'\, \Re(E,E') \\ &\simeq N_{\text{tot}} \sum_{i=1}^{N_{\max}} P(E_i) 2\Delta \int_{E_j-\Delta}^{E_j+\Delta} \mathrm{d}E'\, \Re(E_i,E') \\ &= \sum_{i=1}^{N_{\max}} N_i W_{ij} \end{aligned} \tag{6}$$

where $E_{\max}$ is the maximum spectrum energy, $N_{\max}$ is the maximum number of spectral energy bins, and the *spreading vector* is

$$\begin{aligned} W_{ij} = W_{ji} = W_{|i-j|} &= \frac{1}{\sqrt{2\pi}\sigma} \\ &\times \int_{E_j-\Delta}^{E_j+\Delta} \exp\left[-\frac{1}{2}\left(\frac{E_i-E'}{\sigma}\right)^2\right] \mathrm{d}E' \\ &= \frac{1}{2}\left\{\operatorname{erf}\left(\frac{E_j+\Delta-E_i}{\sqrt{2}\sigma}\right) \right. \\ &\left. -\operatorname{erf}\left(\frac{E_j-\Delta-E_i}{\sqrt{2}\sigma}\right)\right\}. \end{aligned} \tag{7}$$

For the simulated measured spectra shown below, a standard deviation of $\sigma = 20\,\text{keV}$, typical of that for a silicon detector, was assumed.

4. Results

Figs. 5–8 show the simulation results for four thicknesses of a B_4C film, namely, 0.02, 0.27, 2, and 10 μm. Figs. 5 and 6 show the expected results for thin-film-coated B_4C devices and Fig. 8 shows the expected results for B_4C solid-form devices. The progressive change in the differential pulse-height spectrum as the thickness of the B_4C layer increases can be clearly seen in Figs. 5 and 8. From Fig. 5, it is clear that thin B_4C-layers (the 0.02 and 0.27 μm cases) will produce four prominent energy peaks as expected from Eq. (1), and as has been demonstrated experimentally elsewhere [2,11–14]. As the B-layer thickness is increased, the widths of the four peaks become increasingly broader as a direct result of greater ion-energy self-absorption in the film, until finally they are no longer apparent, as seen for the 2 and 10 μm cases. The total counts for the thin-film-coated device increased only slightly for the 10-μm B_4C coating as compared to the 2-μm B_4C coating, a consequence

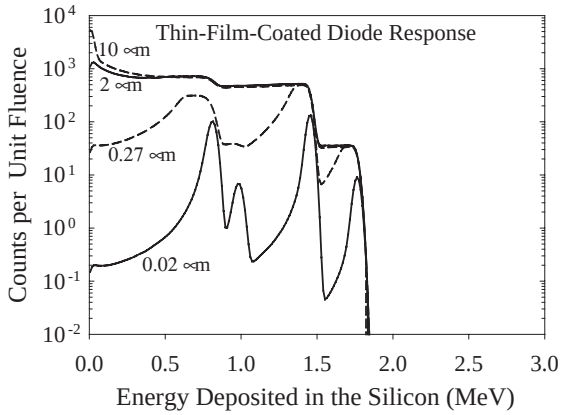

Fig. 5. Simulated differential pulse-height spectra for Si diodes coated with different layer thicknesses of B_4C. The four reaction product energies are clearly visible for the 0.02 and 0.27 μm films.

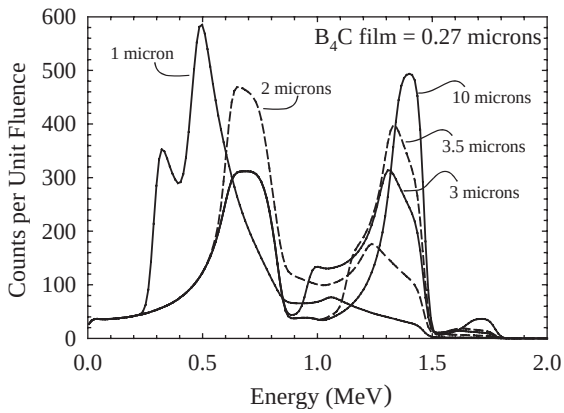

Fig. 6. Simulated differential pulse-height spectra for Si diodes coated with 0.27 μm of B_4C as a function of diode depletion width. Distorted spectra are apparent for diode depletion widths smaller than the maximum range of the $^{10}B(n,\alpha)^7Li$ reaction products, that being 6.3 μm in Si for this example.

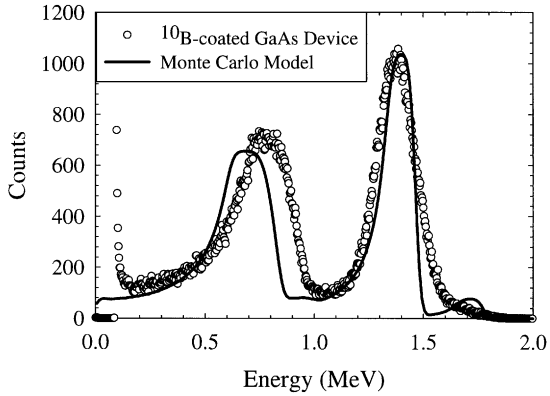

Fig. 7. Comparison spectra between a high-purity GaAs pin diode, with a measured 5 μm wide active region, coated with 0.5 μm of 98% enriched ^{10}B [11,12] and the Monte Carlo model for the 10 μm depleted Si diode coated with 0.27 μm of B_4C. In both cases, the width of the active region is greater than the $^{10}B(n,\alpha)^7Li$ reaction product ranges. The Monte Carlo results were normalized to give the same 1.47 alpha particle peak height as in the GaAs detector data. The resemblance between the spectra is unmistakable, although the detector materials, both the film and the substrates, were different.

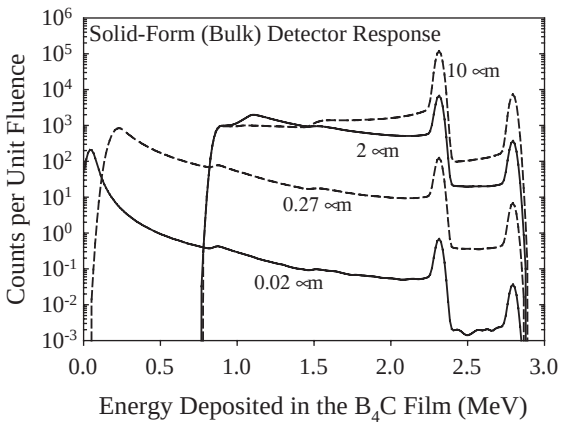

Fig. 8. Simulated differential pulse-height spectra for B_4C solid-form detectors. The two peaks shown on each plot correspond to the total Q-values of the two $^{10}B(n,\alpha)^7Li$ reaction decay branches (2.31 and 2.79 MeV).

of both neutron beam attenuation and reaction product self-absorption effects [2].

The effect of the width of the depletion region in the Si diode on the differential pulse-height spectra for thin-film-coated diodes can be seen in Fig. 6, which shows simulated spectra for a 0.27-μm thick B_4C film upon an Si diode operated with different depletion widths. Since the average range of the highest energy reaction product, the 1.77 MeV alpha particles, in Si is 6.3 μm (from Ref. [10]), the depletion region should extend at least as far to absorb the total energy of all of the reaction products radiating from the B_4C film. A distorted spectrum occurs for depletion widths less than 6.3 μm as a result of incomplete energy deposition in the depletion region. Note also that multiple peaks occurring at energies lower than the full depletion cases shown in Fig. 5 can result, as observed experimentally elsewhere [13].

The simulated Si diode spectrum for the 10-μm depletion width matches quite well with experimental results [11,12], as shown in Fig. 7. The experimental data was taken with a high-purity GaAs p–i–n junction diode coated with 98% enriched ^{10}B [12,13]. The ^{10}B coating for the diode was 0.5 μm, hence causing the peak resolution to be slightly degraded compared to the 0.27-μm-coated case used for the model in Fig. 6. Furthermore, the active depletion width for the GaAs diode was 5 μm [12,13], which is approximately equal to the largest ion range in GaAs, namely 5.2 μm for 1.78 MeV alpha particles. Despite these differences, the model matches well to the experimental results. The observed spectral features are distinctively similar despite boron film composition differences and semiconductor substrate differences. Since the Monte Carlo model approximates the reaction product energy deposited in the semiconductor, regardless of type, the modeled results shown in the present work are valid for a variety of B-based thin-film-coated semiconductor neutron detectors.

Unlike the thin-film-coated diode cases of Figs. 5 and 6, the solid-form device produces only two distinctive "sum" peaks (see Fig. 8). For the thin-film cases (0.02 and 0.27 μm) both energy peaks are significantly lower in total counts and are at higher energies than those in the thin-film-coated device features. The two sum peaks arise from absorption of the total Q value energy of the two $^{10}B(n,\alpha)^7Li$ reaction decay branches, those being 2.79 MeV (6.3%) and 2.31 MeV (93.7%). As shown in Fig. 8, thicker B_4C solid-form devices have larger full energy peaks. Contrary to the

thin-film-coated diode case, the enhanced neutron absorption (of the thicker film) and subsequent capture of the total combined energies from the $^{10}B(n,\alpha)^{7}Li$ reaction products enhance the two energy peaks in a solid-form detector. The long tail regions below the two peaks are from reaction products escaping the device and not depositing their total energy, a similar phenomenon to the "wall effect" for gas-filled neutron detectors [1]. Hence, an energy continuum is observed extending from the sum peaks down to each emission energy of the reaction products.

The contrary energy spectra of thin-film and solid form semiconductor neutron detectors are quite analogous to pulse-height spectra observed with gas-filled neutron detectors. A thin-film-coated detector produces a spectrum very similar to that for a boron-lined proportional gas tube [1], and the solid-form device produces a spectrum similar to a BF_3-gas-filled proportional tube [1]. Indeed, the spectra for the two solid-state device types are almost identical to their gas-filled detector counterparts.

From the results presented here, we observe that spectral results published elsewhere on a thin (0.27 μm) boron-carbide mixture appear to closely resemble the thin-film-coated device model of Fig. 5 rather than the solid-form model of Fig. 8 [6]. Although claimed as solid-form devices in the literature [6], the authors of the present work observe that because the reported boron-carbide films were grown upon n-type Si with a CVD technique [6], it is more likely that the fabrication process has resulted in the production of nothing more than a simple coated p–n junction Si diode, a repeat of an earlier misinterpretation [5]. The modeled results presented in the present communication support such an argument.

5. Conclusions

A model for estimating energy-deposition pulse-height spectra from thin-film-coated and solid-form semiconductor neutron detectors has been presented. Only limited experimental success has been reported for boron-based solid-form semiconductor detectors [15], thereby making a direct comparison of the modeled results in the present work with experimentally observed results problematic. However, the model correctly reproduces spectra observed experimentally for thin-film-coated semiconductor diodes. Furthermore, the model closely reproduces spectra commonly observed from gas-filled devices analogous to the semiconductor devices (B-lined tubes and BF_3-filled tubes). Hence, the modeled results are believed to accurately portray the expected pulse-height spectra from semiconductor-based neutron detectors, both the thin-film-coated and the solid-form configurations. The very different spectra for each detector type can thus be used to assist in the correct interpretation of experimental results from semiconductor-based thermal-neutron detectors.

The authors note that the models presented assume excellent charge collection properties of the semiconductors, be it coated-diodes or solid-form devices. Unfortunately, most experimental compound semiconductors suffer significant charge carrier trapping which ultimately results in poor energy resolution of the spectral features. Although some mature semiconductors, such as Si and GaAs, have demonstrated excellent energy resolution for thin-film-coated diodes, the same may not be true for boron-based semiconductor compounds. Hence, what are presented here are the best possible results. In the presence of marginal-quality semiconductor materials, such as amorphous or polycrystalline B-based materials, it is expected that the spectral features will become distorted with much broader energy peaks [15]. In instances with severe charge carrier transport problems, no spectral features may be observed. However, if spectral features are observed, it becomes readily apparent that proper interpretation of the data, as presented in the present work, becomes a valuable tool for identifying the type of neutron detector developed.

References

[1] G.F. Knoll, Radiation Detection and Measurement, 3rd Edition, Wiley, New York, 2000.
[2] D.S. McGregor, M.D. Hammig, H.K. Gersch, Y-H. Yang, R.T. Klann, Nucl. Instr. and Meth. A 500 (2003) 272.

[3] T.L. Chu, A.E. Hyslop, J. Electrochem. Soc. 43 (1974) 412.
[4] Y. Kumashiro, J. Mater. Res. 5 (1990) 2933.
[5] J.C. Lund, F. Olschner, F. Ahmed, K.S. Shah, Proc. MRS 162 (1990) 601.
[6] B.W. Robertson, S. Adenwalla, A. Harken, P. Welsch, J.I. Brand, P.A. Dowben, J.P. Classen, Appl. Phys. Lett. 80 (2002) 3644.
[7] S. Wolf, R.N. Tauber, Silicon Processing, Lattice Press, Sunset Beach, 1986.
[8] R.C. Jaeger, Introduction to Microelectronic Fabrication, Addison-Wesley, Reading, MA, 1993.
[9] C.R. Hammond, in: R.C. Weast (Ed.), Handbook of Chemistry and Physics, 58th Edition, CRC Press, West Palm Beach, 1978.
[10] J.F. Ziegler, J.P. Biersack, TRIM, SRIM-2000.40 Code, Version 9, IBM Company, 1998.
[11] D.S. McGregor, H.K. Gersch, J.D. Sanders, R.T. Klann, J.T. Lindsay, J. Korean Assoc. Radiat. Prot. 26 (2001) 167.
[12] H.K. Gersch, D.S. McGregor, P.A. Simpson, Nucl. Instr. and Meth. A 489 (2002) 85.
[13] D.S. McGregor, S.M. Vernon, H.K. Gersch, S.M. Markham, S.J. Wojtczuk, D.K. Wehe, IEEE Trans. Nucl. Sci. NS-47 (2000) 1364.
[14] D.S. McGregor, R.T. Klann, H.K. Gersch, Y–H. Yang, Nucl. Instr. and Meth. A 466 (2001) 126.
[15] F.P. Doty, I. Zwieback, W. Ruderman, US Patent 6,388,260, issued May 14, 2002.